$\bar{K}$ nuclear bound states in a dynamical model

J. Mareš,[1,*] E. Friedman,[2,†] and A. Gal[2,‡]

[1] *Nuclear Physics Institute, 25068 Řež, Czech Republic*

[2] *Racah Institute of Physics, The Hebrew University, Jerusalem 91904, Israel*

(Dated: February 9, 2008)

A comprehensive data base of K^--atom level shifts and widths is re-analyzed in order to study the density dependence of the $\bar{K}$-nuclear optical potential. Significant departure from a $t_{\rm eff}\rho$ form is found only for $\rho(r)/\rho_0 \lesssim 0.2$ and extrapolation to nuclear-matter density ρ_0 yields an attractive potential, about 170 MeV deep. Partial restoration of chiral symmetry compatible with pionic atoms and low-energy pion-nuclear data plays no role at the relevant low-density regime, but this effect is not ruled out at densities of order ρ_0 and beyond. $\bar{K}$-nuclear bound states are generated across the periodic table self consistently, using a relativistic mean-field model Lagrangian which couples the $\bar{K}$ to the scalar and vector meson fields mediating the nuclear interactions. The reduced phase space available for $\bar{K}$ absorption from these bound states is taken into account by adding an energy-dependent imaginary term which underlies the corresponding $\bar{K}$-nuclear level widths, with a strength required by fits to the atomic data. Substantial polarization of the core nucleus is found for light nuclei, and the binding energies and widths calculated in this dynamical model differ appreciably from those calculated for a static nucleus. A wide range of binding energies is spanned by varying the $\bar{K}$ couplings to the meson fields. Our calculations provide a lower limit of $\Gamma_{\bar{K}} = 50 \pm 10$ MeV on the width of nuclear bound states for $\bar{K}$ binding energy in the range $B_{\bar{K}} \sim 100 - 200$ MeV. Comments are made on the interpretation of the FINUDA experiment at DAΦNE which claimed evidence for deeply bound K^-pp states in light nuclei.

PACS numbers: 13.75.Jz; 21.30.Fe; 25.80.Nv; 36.10.Gv

Keywords: Kaonic atoms; $\bar{K}$ nuclear bound states; Density-dependent $\bar{K}$-nucleus interaction; $\bar{K}$ nuclear relativistic mean-field calculations

*Electronic address: mares@ujf.cas.cz

†Electronic address: elifried@vms.huji.ac.il

‡Electronic address: avragal@vms.huji.ac.il

I. INTRODUCTION

The existence of a $\bar{K}N$ unstable bound state, the $I = 0$ $\Lambda(1405)$ $\pi\Sigma$ resonance, about 27 MeV below the K^-p threshold was first discussed by Dalitz et al. [1] and shown to be compatible with strong coupled-channel vector-meson exchange s-wave interactions in the $I = 0$ $\bar{K}N$ $-$ $\pi\Sigma$ system. This strongly attractive $I = 0$ $\bar{K}N$ interaction, plus the moderately attractive $I = 1$ $\bar{K}N$ interaction [2], suggest that the $\bar{K}$-*nuclear* interaction is also strongly attractive. Indeed, the Born approximation for the $\bar{K}$-nucleus optical potential constructed from the leading-order Tomozawa-Weinberg (TW) vector coupling term of the chiral effective Lagrangian [3],

$$V_{\rm opt}^{\bar{K}} \;=\; -\,\frac{3}{8f_\pi^2}\,\rho \tag{1}$$

where $f_\pi \sim 93$ MeV is the pseudoscalar meson decay constant, yields sizable attraction $V_{\rm opt}^{\bar{K}} \sim -55$ MeV for a central nuclear density $\rho \sim \rho_0 = 0.16$ fm^{-3}. Iterating the TW term plus next-to-leading-order terms, within an *in-medium* coupled-channel approach constrained by the $\bar{K}N - \pi\Sigma - \pi\Lambda$ data near the $\bar{K}N$ threshold, roughly doubles this $\bar{K}$-nucleus attraction to about -110 MeV at ρ_0. It is found in these calculations (e.g. [4]) that the $\Lambda(1405)$ quickly dissolves in the nuclear medium at finite densities, well below ρ_0, so that the repulsive free-space scattering length a_{K^-p} becomes *attractive*, and together with the weakly density dependent attractive a_{K^-n} it yields a strongly attractive density-dependent '$t\rho$' $\bar{K}$-nucleus optical potential:

$$V_{\rm opt}^{\bar{K}}(r) \;=\; -\,\frac{2\pi}{\mu_{KN}} b_0(\rho)\rho(r)\ , \tag{2}$$

where μ_{KN} is the $\bar{K}N$ reduced mass and the in-medium isoscalar $\bar{K}N$ scattering length $b_0(\rho)$ (positive for attraction in the sign convention common in this field) is defined by

$$b_0(\rho) = \frac{1}{2}(a_{K^-p}(\rho) + a_{K^-n}(\rho))\ , \quad b_0(\rho_0) \sim 0.9 \text{ fm}\ . \tag{3}$$

However, when $V_{\rm opt}^{\bar{K}}$ is calculated *self consistently*, namely by including $V_{\rm opt}^{\bar{K}}$ in the in-medium propagator used in the Lippmann-Schwinger equation determining $V_{\rm opt}^{\bar{K}}$ as a $\bar{K}$-nucleus T matrix, the resultant $\bar{K}$-nucleus potential is only moderately attractive, with depth between 40 and 60 MeV [5, 6, 7]. We call such $\bar{K}$-nucleus potentials 'shallow'. In contrast, strongly attractive $\bar{K}$-nucleus potentials, of depth between 150 and 200 MeV, appear to provide the best fit to the comprehensive K^- atomic data which consist of level shifts and widths across the periodic table [8, 9, 10]. We call such $\bar{K}$-nucleus potentials 'deep', noting that the fits provided by such 'deep' potentials to the K^- atomic data are by far superior to those provided by the 'shallow' potentials [7].

Another approach to the construction of $V_{\rm opt}^{\bar{K}}$ in dense nuclear matter has been the relativistic-mean-field (RMF) approach where in addition to an attractive Lorentz-vector mean potential, similar in its origin to Eq. (1), an attractive Lorentz-scalar mean potential associated with the poorly known sigma term is included [11, 12, 13, 14]. This approach

too yields a strongly attractive $V_{\rm opt}^{\bar K}$, the precise extent of attraction depending on the phenomenological constraints imposed on the RMF calculation. Assuming dominance of the Lorentz-vector mean potential proportional to f_π^{-2}, one could test the implications of partial restoration of chiral symmetry, in the sense originally proposed for pionic atoms [15], by replacing in Eq. (1) f_π by a density dependent decay constant f_π^* according to

$$f_\pi^{*2} = f_\pi^2 - \frac{\sigma}{m_\pi^2}\rho \quad , \tag{4}$$

where σ is the pion-nucleon sigma term [16]. This implies a specific density dependence of the optical potential (2):

$$b_0(\rho) \;=\; \frac{b_0(0)}{1 \;-\; 0.046\sigma\rho} \tag{5}$$

where the πN σ term is given in MeV and ρ is the nuclear density in fm^{-3}. This chirally motivated density dependence has proved successful in pionic atoms [17, 18, 19, 20, 21, 22] and in low energy pion scattering [23, 24] where its effect can be separated from similar effects due to the threshold energy dependence of the underlying πN amplitudes [21, 23].

The $\bar K$-nuclear interaction is also strongly absorptive, which arises from the available one-nucleon absorption reactions $\bar K N \to \pi Y$ with approximately 100 and 180 MeV energy release for the final hyperons (Y) Σ and Λ, respectively. Among the known hadron-nucleus interactions at low energies, only the $\bar N$-nucleus interaction is as strongly attractive and absorptive as the $\bar K$-nucleus interaction [25].

Recent experimental reports on candidates for $\bar K$-nuclear deeply bound states in the range of binding energy $B_{\bar K} \sim 100 - 200$ MeV [26, 27, 28, 29] again highlighted the question of how attractive the $\bar K$-nucleus interaction is below the $\bar K N$ threshold. Obviously, the 'shallow'-type potentials cannot generate deeply bound nuclear states in the energy range $B_{\bar K} \sim 100 - 200$ MeV, whereas the 'deep' potentials might do. The distinction between 'deep' and 'shallow' $\bar K$-nucleus potentials becomes somewhat fuzzy within a *dynamical* approach which allows for polarization of the nucleus by the strong $\bar K$-nucleus interaction. The depth of the $\bar K$-nucleus potential becomes then state dependent, thus depending on the binding energy $B_{\bar K}$. Indeed, strong polarization of the nucleus by the $\bar K$ interaction was established in our recent RMF calculations for the light nuclei ^{12}C and ^{16}O [30]. Consequences of such polarization are a central topic of the present work.

In Section 2 we re-analyze the existing K^- atomic data in order to gain information on the density dependence of the $\bar K$-nuclear optical potential in the nuclear surface and to extrapolate smoothly to nuclear matter density. This procedure yields a 'deep' attractive potential of about 170 MeV at ρ_0. We also test whether starting from a 'shallow'-type potential [5, 6, 7], and superimposing on it a density dependence of the form Eq. (5), could improve the fit to the K^--atom data as it appears to do in pionic atoms and in low-energy pion-nuclear scattering [17, 18, 19, 20, 21, 22, 23, 24]. For K^- atoms the answer is in the negative, perhaps because the nonperturbative aspect of the $\Lambda(1405)$ dominance at the low density regime encountered in kaonic atoms invalidates the chiral perturbation counting rules

[31]. This does not rule out a greater role for partial chiral restoration of a similar sort at higher densities, and for deeply bound $\bar{K}$-*nuclear* states, or for kaon condensation as discussed first by Brown et al. [32].

The case for $\bar{K}$-nucleus bound states with $B_{\bar{K}} \sim 100$ MeV, generated by a 'deep' potential, was made by Akaishi and Yamazaki [33] who fitted the underlying t matrix to a *partial* set of the available low-energy $\bar{K}N$ data. For the most recent publication that elaborates on their calculations for very light nuclear cores, see Ref. [34]. In these few-body calculations, the strongly attractive $\bar{K}$-nucleus interaction caused a substantial polarization, or rearrangement of the nuclear core. In our *dynamical* RMF calculations [30], the $\bar{K}$ and the nucleons interact through the exchange of scalar (σ) and vector (ω) meson fields which are treated in the mean-field approximation. The presence of $\bar{K}$ induces additional source terms in the equations of motion for the meson fields to which the $\bar{K}$ couples. This affects the scalar and vector potentials which enter the Dirac equation for nucleons and leads to rearrangement of the nuclear core. It also leads to a deeper $\bar{K}$-nuclear potential with respect to *static* calculations which assume a rigid nuclear core (an assumption that is justified for K^- and $\bar{p}$ atoms [30, 35]). By successively allowing the $\bar{K}$ to polarize the nucleons, and the polarized nucleus to enhance the $\bar{K}$-nuclear interaction, this dynamical calculation is made self consistent. Similar $\bar{N}$-nucleus RMF calculations have been reported by the Frankfurt group [36, 37].

In the present paper we extend the results of Ref. [30] in order to study the dynamical aspects of the $\bar{K}$-nucleus coupling across the periodic table, and in particular to study the widths expected for deeply bound states over a wide range of binding energies. This is done by scanning on the coupling constants of the $\bar{K}$ - meson fields. In Section 3 we outline the $\bar{K}$-nucleus RMF methodology used in this work and discuss its extension to describe absorptive interactions by which the $\bar{K}$-nuclear bound states acquire a width. The calculation of the width is also done dynamically, since its evaluation requires the nonstatic nuclear density and the binding energy which determines the reduced phase space available to the absorption reactions, and both of these quantities keep changing from one step of the iterative solution of the equations of motion to the next. The imaginary part of the potential affects also nonnegligibly the calculated binding energy. This important aspect of the $\bar{K}$-nucleus dynamics is missing in the very recent RMF calculation by Zhong et al. [38]. In Section 4 we show and discuss the results of calculations across the periodic table. Special attention is paid to ^{12}C and other light nuclear targets for which a recent FINUDA experiment at DAΦNE, Frascati, claimed evidence for deeply bound K^-pp states [29]. We find large dynamical effects for light nuclei such as ^{12}C and we discuss these in detail. Section 5 summarizes the present work with conclusions and outlook.

II. KAONIC ATOMS

A. Motivation and background

As explained in the Introduction, the motivation for re-analysis of a comprehensive set of kaonic atoms data is two fold. First is the question of 'deep' *vs.* 'shallow' real $\bar{K}$-nucleus potential, in light of recent possible experimental evidence for the existence of deeply bound kaonic states whose binding energies exceed the depth of the shallow type of potential obtained from fits to kaonic atoms data. Such shallow potentials are obtained when fits to the data are made with a simple '$t\rho$' approach, as described below, and also when self-consistent approaches are used [5, 6, 7]. However, if the deep variety of potential is confirmed, then the dependence of the $\bar{K}N$ interaction on the nuclear density becomes of prime concern. This density dependence is the second point which motivated the re-analysis of kaonic atoms data although there have not been any new experimental results on strong interaction effects in kaonic atoms since the early 1990's.

The method adopted here is rather similar to our earlier work [8, 9, 10], namely, performing global fits to a large set of data which covers the whole of the periodic table, using an optical potential within the Klein-Gordon equation,

$$\left[\Delta - 2\mu(B + V_{\rm opt} + V_c) + (V_c + B)^2\right]\psi = 0 \quad (\hbar = c = 1), \tag{6}$$

where V_c denotes the static Coulomb potential for the $\bar{K}$ due to the finite charge distribution of the nucleus, including the first-order $\alpha(Z\alpha)$ vacuum-polarization potential, μ is the $\bar{K}$-nucleus reduced mass and $B = B_{\bar{K}} + {\rm i}\Gamma_{\bar{K}}/2$, with $B_{\bar{K}}$ and $\Gamma_{\bar{K}}$ standing for the binding energy and width, respectively. The interaction of $\bar{K}$ with the nucleus is described here in terms of an optical potential $V_{\rm opt}$ which in the simplest '$t\rho$' form is given by

$$2\mu V_{\rm opt}(r) = -4\pi(1 + \frac{\mu}{m_N}\frac{A-1}{A})b_0(\rho_n(r) + \rho_p(r)) \quad , \tag{7}$$

where ρ_n and ρ_p are the neutron and proton density distributions normalized to the number of neutrons N and number of protons Z, respectively, $A = N + Z$, and m_N is the mass of the nucleon. In the impulse approximation '$t\rho$' approach the parameter b_0 is equal to the $\bar{K}$-nucleon isoscalar scattering length under the sign convention common in this field, otherwise this parameter may be regarded as 'effective' and its value is obtained from fits to the data. For $A >> 1$, Eq. (7) reduces to Eq. (2) discussed above in the context of nuclear matter. An isovector term is not included in Eq. (7) as earlier analyses showed [10] that such a term is not required by fits to kaonic atoms data. Compared to the previous analyses we have now used a modified set of parameters for the nuclear densities. The density distribution of the protons is usually considered known as it is obtained from the nuclear charge distribution by unfolding the finite size of the charge of the proton. The neutron distributions are, however, generally not known

to sufficient accuracy. Experience with pionic atoms [20] and with antiprotonic atoms [35] showed that the feature of neutron density distributions which is most relevant in determining strong interaction effects in exotic atoms is the radial extent, as represented for example by r_n, the neutron density rms radius. Other features such as the detailed shape of the distribution have only minor effect. This is observed also for kaonic atoms where the dependence of the quality of fits on the densities of the neutrons is less than what is observed for pionic and antiprotonic atoms. The neutron densities used in the present work were of the two-parameter Fermi shape and of the 'skin' variety, as detailed in Ref. [35]. The values of r_n were those that yielded the best fit to pionic and antiprotonic atoms data.

With the potential Eq. (7) and varying the complex parameter b_0 we obtain the same results as before [10] when the data span a range of nuclei from ^{7}Li to ^{238}U. The value of χ^2 is marginally larger than the corresponding value found in [10] because of the slightly different nuclear densities used in the two calculations. The depth of the real potential for a typical medium-weight to heavy nucleus is about 80 MeV. Recall that the corresponding value for the shallow-type potentials is close to 55 MeV [7].

B. Density dependence

The possibility of departure of the antikaon-nucleus potential from the simple '$t\rho$' form had been studied over a decade ago [8, 9, 10] and significant improvement in the fit to the data had been achieved. The empirical parameter b_0 was made density dependent (DD) by replacing b_0 in Eq. (7) by

$$b_0 \ \rightarrow b_0 \ + \ B_0 \ [\frac{\rho(r)}{\rho_0}]^\alpha \tag{8}$$

where $\rho_0 \ = \ 0.16$ fm^{-3}. In this way it was possible to respect the 'low density limit' (when $\alpha > \ 0$) by keeping b_0 fixed at its free $\bar{K}N$ value and varying the parameters B_0 and α. In view of the importance of the modification of the $\bar{K}N$ interaction in nuclear matter we have addressed this question again in the present work in a different way.

We *loosely* define in coordinate space an 'internal' region and an 'external' region by using the multiplicative functions $F(r)$ in the former and $[1 - F(r)]$ in the latter, where $F(r)$ is defined as

$$F(r) \ = \ \frac{1}{e^x + 1} \tag{9}$$

with $x \ = \ (r - R_x)/a_x$. Then clearly $F(r) \ \rightarrow \ 1$ when $r \ < \ R_x \ - \ 3 \ a_x$, which is the internal region. Likewise $[1 \ - \ F(r)] \ \rightarrow \ 1$ in the external region. Thus R_x forms an approximate border between the internal and the external regions, and *if* R_x is close to the nuclear surface then the two regions will correspond to the high density and low density regions of nuclear matter, respectively. We have therefore replaced the fixed b_0 in the $t\rho$ potential Eq. (7) by

$$b_0 \ \rightarrow \ B_0 \ F(r) \ + \ b_0 \ [1 \ - \ F(r)] \ . \tag{10}$$

TABLE I: Parameter values from global fits to kaonic atoms data, for the models of Eqs. (7)-(10). Additional parameters for the fit using Eq. (10) are $R_{x0} = 1.30 \pm 0.05$ fm, $\delta_x = 0.8 \pm 0.3$ fm, a_x=0.4 fm. Underlined parameter values were held fixed in the fit process. χ^2 values are for 65 data points, b_0 and B_0 are in units of fm.

potential	χ^2	Reb_0	Imb_0	ReB_0	ImB_0	α
Eq. (7) ('$t\rho$')	129.4	0.62±0.05	0.92±0.05	-	-	-
Eq. (8) ('DD')	103.3	$\underline{-0.15}$	$\underline{0.62}$	1.62±0.07	−0.02±0.02	0.24±0.03
Eq. (10) ('F')	84.4	$\underline{-0.15}$	$\underline{0}$	1.42±0.05	0.66±0.05	-

Here the parameter b_0 represents the large-r interaction, and it can be held fixed, e.g. at the free $\bar{K}N$ value. The parameter B_0 represents the interaction inside the nucleus. As stated above, this division into regions of high and low densities is meaningful *provided* R_x is close to the radius of the nucleus and a_x is of the order of 0.5 fm. To enable global fits to be made over the whole of the periodic table we parameterized R_x as $R_x = R_{x0}\, A^{1/3} + \delta_x$ and varied in the least-squares fit the values of B_0, R_{x0} and δ_x while gridding on values of a_x. The parameter Reb_0 was held fixed at its free $\bar{K}N$ value but the results depend very little on its precise value.

Table I shows results of χ^2 fits to kaonic atoms data over the whole of the periodic table using the three potentials described above. For the third option, Eq. (10), the values of the geometrical parameters for $a_x = 0.4$ fm are found to be $R_{x0} = 1.30 \pm 0.05$ fm, $\delta_x = 0.8 \pm 0.3$ fm, implying that the modification of the free $\bar{K}N$ interaction takes place at radii somewhat outside of the nuclear 'half-density' radius. Changing the value of a_x between 0.2 and 0.5 fm made no difference. The ansatz Eq. (10) was applied to both real and imaginary parts of B_0, otherwise the fit deteriorates.

Figure 1 shows the real part of the $\bar{K}$-nucleus potential for ^{58}Ni and ^{208}Pb for the $t\rho$ model and for the two density-dependent potentials described above. The difference between the relatively shallow $t\rho$ potential and the deep potentials is clearly seen. Figure 2 shows similar results for the imaginary part of the potential. Although the two density-dependent potentials have very different parameterizations the resulting potentials are quite similar.

In Figure 3 are plotted the $F(r)$ functions for ^{58}Ni and ^{208}Pb, not as functions of r but rather as *functionals* of the local nuclear density ρ, which is of prime interest in the present work. We note that for these two examples, representing medium-weight and heavy nuclei, the two curves are very close to each other. The two vertical dotted lines represent 10% and 50% of a nuclear matter density of 0.16 fm^{-3}. It is evident that the potential departs from the $\rho(r)$ dependence for density lower than about 20% of its central value.

Finally, we have tried to fit the K^- atoms data with the density dependence given by Eq. (5) as a possible signature of partial restoration of chiral symmetry in dense nuclear medium [15]. However, no improvement on the shallow $t\rho$ potential for K^- atoms was achieved when starting from the self-consistent amplitudes of Ramos and Oset [6] using for σ values around 50 MeV [16]. That is in line with Fig. 3 where it is seen empirically that the density dependence

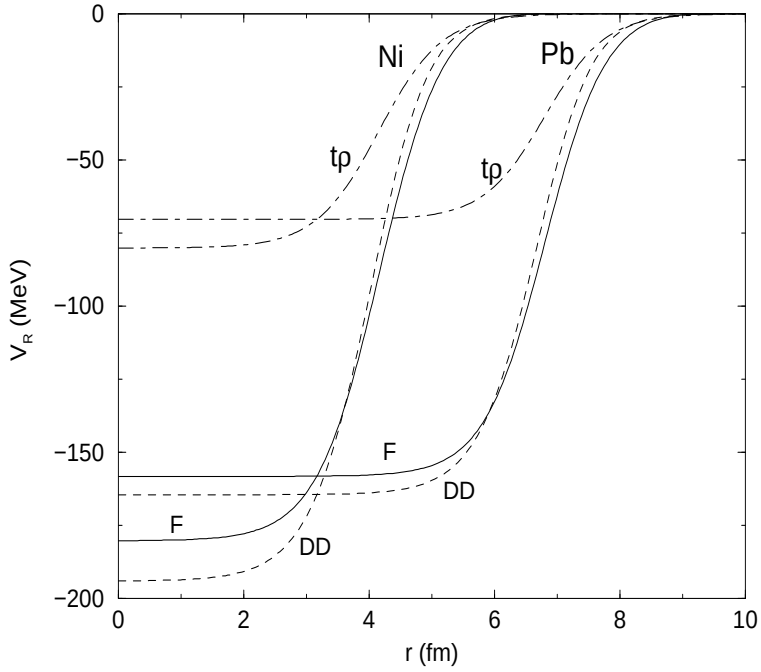

FIG. 1: Real part of the $\bar{K}$-nucleus potential for ^{58}Ni and ^{208}Pb, for the $t\rho$ model ($t\rho$, dash-dots), for the DD potential of Eq. (8) (DD, dashed) and for the potential of Eq. (10) (F, solid curves).

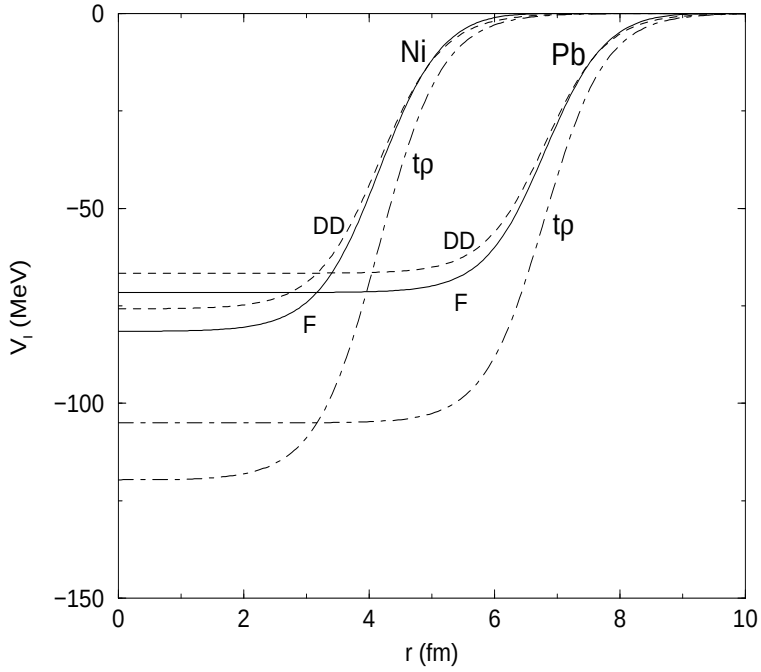

FIG. 2: Same as Fig. 1 but for the imaginary part of the $\bar{K}$-nucleus potential.

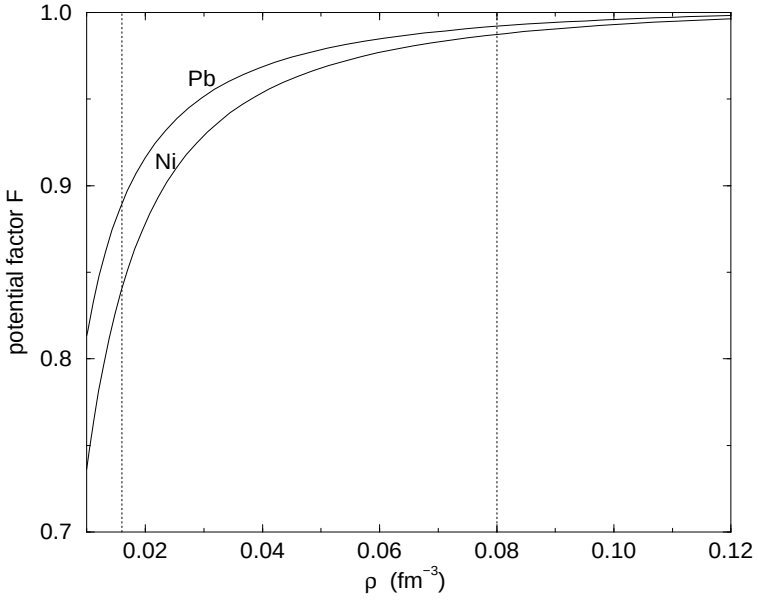

FIG. 3: The modifying factor F, Eq. (9), as a functional of ρ, see text. The vertical dotted lines indicate 10% and 50% of nuclear matter density $\rho_0 = 0.16$ fm^{-3}.

is effective only at fairly low densities, considerably lower than the ones reached in pionic atoms ($\sim 0.5\ \rho_0$).

III. $\bar{K}$ NUCLEAR RMF METHODOLOGY

The theoretical framework adopted in this work for calculating $\bar{K}$ nuclear bound states is the relativistic mean field (RMF) model for a system of nucleons and one $\bar{K}$ meson [30]. In this model, the interactions between hadrons are mediated by the exchange of scalar and vector boson fields which are treated in the mean-field approximation. In the calculations reported in Ref. [30] and extended here, we employed the standard RMF Lagrangian $\mathcal{L}_N$ for the description of the nucleon sector, with the linear parameterization L-HS of Horowitz and Serot [39], as well as with several nonlinear parameterizations, but mostly NL-SH due to Sharma et al. [40]. These parameterizations give quite different values for the nuclear compressibility and, therefore, are expected to provide different rearrangement of the nuclear core due to the presence of $\bar{K}$. The (anti)kaon interaction with the nuclear medium is incorporated by adding to $\mathcal{L}_N$ the Lagrangian density $\mathcal{L}_K$ [11, 12]:

$$\mathcal{L}_K = \mathcal{D}^*_\mu \bar{K} \mathcal{D}^\mu K - m_K^2 \bar{K} K - g_{\sigma K} m_K \sigma \bar{K} K \ . \tag{11}$$

The covariant derivative $\mathcal{D}_\mu = \partial_\mu + i g_{\omega K} \omega_\mu$ describes the coupling of the (anti)kaon to the vector meson ω. The vector field ω is then associated with a conserved current. The coupling of the (anti)kaon to the isovector ρ meson is here excluded. This is a good approximation for $N = Z$ nuclei which holds for the majority of nuclei considered

here, but not necessarily for the heavier ^{208}Pb nucleus. We note in this respect that optical-potential fits as described in Sect. II for kaonic atoms, including data for nuclei with excess neutrons up to ^{238}U, found no need to introduce isovector components.

Whereas extending the nuclear Lagrangian $\mathcal{L}_N$ by the Lagrangian $\mathcal{L}_K$ does not affect the original form of the corresponding Dirac equation for nucleons, the presence of $\bar{K}$ induces additional source terms in the equations of motion for the meson fields σ and ω_0 to which the $\bar{K}$ couples:

$$\left(-\Delta + m_\sigma^2\right)\sigma \;\; = \;\; -g_{\sigma N}\rho_S - g_{\sigma K} m_K \bar{K} K + \left(-g_2\,\sigma^2 - g_3\,\sigma^3\right) \;, \tag{12}$$

$$\left(-\Delta + m_\omega^2\right)\omega_0 \;\; = \;\; +g_{\omega N}\rho_V - 2g_{\omega K}(\omega_K + g_{\omega K}\omega_0)\bar{K} K \;, \tag{13}$$

where ω_K is the $\bar{K}$ energy in the nuclear medium:

$$\omega_K = \sqrt{m_K^2 + g_{\sigma K} m_K \sigma + p_K^2} - g_{\omega K}\omega_0 \;,$$

and ρ_S and ρ_V denote the nuclear scalar and vector densities, respectively. The additional source terms due to the $\bar{K}$ in Eqs. (12)-(13) affect the scalar and vector fields (potentials) which enter the Dirac equation for nucleons. This leads to the rearrangement, or polarization of the nuclear core in the presence of $\bar{K}$.

The equation of motion for $\bar{K}$ is derived from the Lagrangian $\mathcal{L}_K$ using standard techniques. In order to preserve the connection to previous studies of kaonic atoms, the corresponding Klein Gordon (KG) equation of motion for the $\bar{K}$ is used in the form of Eq. (6) which is rewritten here

$$\left[\Delta - 2\mu(B^{\rm s.p.} + V_{\rm opt} + V_c) + (V_c + B^{\rm s.p.})^2\right]\bar{K} = 0 \qquad (\hbar = c = 1) \;, \tag{14}$$

where the superscript s.p. in $B^{\rm s.p.} = B^{\rm s.p.}_{\bar{K}} + {\rm i}\Gamma_{\bar{K}}/2$ stands for the single-particle $\bar{K}$ binding energy which is equal to the $\bar{K}$ separation energy only in the static calculation, as elaborated below. Moreover, in this particular form of the KG equation, it admits a straightforward extention, by allowing $V_{\rm opt}$ to become *complex*, to consider dynamically the width $\Gamma_{\bar{K}}$ of $\bar{K}$ nuclear bound states. This is a new and crucial element in our calculations. The real part of the $\bar{K}$ optical potential $V_{\rm opt}$ in Eq.(14) is then given by

$${\rm Re}V_{\rm opt} = \frac{m_K}{\mu}[\frac{1}{2}S - (1 - \frac{B^{\rm s.p.}_{\bar{K}} + V_c}{m_K})V - \frac{V^2}{2m_K}] \;, \tag{15}$$

where $S = g_{\sigma K}\sigma$ and $V = g_{\omega K}\omega_0$ are the scalar and vector potentials due to the σ and ω mean fields, respectively. We note that ${\rm Re}V_{\rm opt}$ is explicitly *state dependent* through the $(1 - [B^{\rm s.p.}_{\bar{K}} + V_c]/m_K)$ energy-dependent factor which multiplies the vector potential. This factor was disregarded in our Letter [30] where the state dependence of ${\rm Re}V_{\rm opt}$ arose only implicitly through the dynamical density dependence of the mean-field potentials S and V.

The binding (separation) energy of $\bar{K}$, $B_{\bar{K}}$, in the combined $\bar{K}$ nuclear system ${}^{A}_{\bar{K}}Z$ is given by

$$B_{\bar{K}} = B({}^{A}_{\bar{K}}Z) - B({}^{A}Z) \ . \tag{16}$$

Here $B({}^{A}Z)$ is the *total* binding energy of the nucleus ${}^{A}Z$. It is to be noted that the total binding energy $B({}^{A}_{\bar{K}}Z)$ of the $\bar{K}$ nucleus, besides including nucleon single-particle energies, mean-field energies and center-of-mass energy, also includes the $\bar{K}$ single-particle binding energy $B^{\rm s.p.}_{\bar{K}}$ from Eq. (14) and the additional meson mean-field contributions from the source terms due to (anti)kaons in the KG Eqs. (12)-(13) for the σ and ω meson fields. Whereas $B_{\bar{K}} = B^{\rm s.p.}_{\bar{K}}$ for the static calculation, $B^{\rm s.p.}_{\bar{K}} > B_{\bar{K}}$ for the dynamical calculation, and this latter difference defines the nuclear rearrangement energy which is related to the polarization of the nuclear core by the $\bar{K}$. These statements are demonstrated in Section IV.

Since the traditional RMF approach does not address the imaginary part of the potential, ${\rm Im}V_{\rm opt}$ was taken in a phenomenological $t\rho$ form, where its depth was fitted to the K^- atomic data [14] and the nuclear density ρ was calculated within the RMF model. We emphasize that ρ in the present calculations is no longer a static nuclear density. Here it is a *dynamical* entity affected by the $\bar{K}$, which is embedded in the nuclear medium and interacts with the nucleons via boson fields. The resulting increased nuclear density leads to increased widths, particularly for deeply bound states. On the other hand, the phase space available for the decay products is reduced for deeply bound states, which will act to decrease the calculated width. Thus, suppression factors multiplying ${\rm Im}V_{\rm opt}$ were introduced from phase-space considerations, taking into account the binding energy of the kaon for the initial decaying state, and assuming two-body final-state kinematics for the decay products. Two absorption channels were considered. The dominant one for absorption at rest is due to pionic conversion modes on a single nucleon:

$$\bar{K}N \to \pi\Sigma, \ \ \pi\Lambda \quad (\sim 80\%) \ , \tag{17}$$

with thresholds about 100 MeV and 180 MeV, respectively, below the $\bar{K}N$ total mass. The corresponding density-independent suppression factor is given by

$$f_1 = \frac{M_{01}^3}{M_1^3}\sqrt{\frac{[M_1^2-(m_\pi+m_Y)^2][M_1^2-(m_Y-m_\pi)^2]}{[M_{01}^2-(m_\pi+m_Y)^2][M_{01}^2-(m_Y-m_\pi)^2]}}\ \Theta(M_1-m_\pi-m_Y) \quad , \tag{18}$$

where $M_{01} = m_K + m_N$, $M_1 = M_{01} - B_{\bar{K}}$. The second channel is due to non-pionic absorption modes on two nucleons:

$$\bar{K}NN \to YN \quad (\sim 20\%) \ , \tag{19}$$

with thresholds about $m_\pi = 140$ MeV lower than the single-nucleon threshold. This second channel represents in our model all the *multi-nucleon* absorption modes which are not resolved by experiment. The corresponding suppression

factor is given by

$$f_2 = \frac{M_{02}^3}{M_2^3}\sqrt{\frac{[M_2^2-(m_N+m_Y)^2][M_2^2-(m_Y-m_N)^2]}{[M_{02}^2-(m_N+m_Y)^2][M_{02}^2-(m_Y-m_N)^2]}}\;\Theta(M_2-m_Y-m_N) \quad , \tag{20}$$

where $M_{02} = m_K + 2m_N,\ M_2 = M_{02} - B_{\bar{K}}$. The branching ratios (quoted above in parentheses) are known from bubble-chamber experiments [41]. Although multi-nucleon absorption modes are often modeled to have a power-law ρ^α ($\alpha > 1$) density dependence, a linear density dependence ($\alpha = 1$) may also arise in multi-step reaction mechanisms [42]. Since our comprehensive K^--atom fits [8] are satisfied with $\alpha \sim 1$, we here assume $\alpha = 1$ which means that f_2 too is independent of density. We comment below on the effect of a possible density dependence of f_2, reflecting perhaps a ρ^2 dependence of the non-pionic decay mode Eq. (19) at high densities.

Since Σ final states dominate both the pionic and non-pionic channels [41], the hyperon Y was here taken as $Y = \Sigma$. Allowing Λ hyperons would foremost *add* conversion width to $\bar{K}$ states bound in the region $B_{\bar{K}} \sim 100 - 180$ MeV. For the combined suppression factor we assumed a mixture of 80% mesonic decay and 20% nonmesonic decay [41], i.e.

$$f = 0.8\ f_1\ +\ 0.2\ f_2\ . \tag{21}$$

In the calculations below, a residual value of $f = 0.02$ was assumed when both f_1 and f_2 vanish.

The coupled system of equations for nucleons and for the electromagnetic vector field A_0, for the ρ meson mean field, and for the mean fields σ and ω_0 Eqs. (12)-(13) above, as well as the KG Eq. (14) for K^-, were solved self consistently using an iterative procedure. Obviously, the requirement of self-consistency is crucial for the proper evaluation of the dynamical effects of the $\bar{K}$ on the nuclear core and vice versa. We note that self consistency is not imposed here on the final-state hadrons which only enter through their *on-shell* masses used in the phase-space suppression factors given above. For the main $\pi\Sigma$ decay channel it is likely that the attraction provided by the pion within a dynamical calculation [6] is largely cancelled by the nuclear repulsion deduced phenomenologically for Σ hyperons [43, 44, 45].

IV. RESULTS AND DISCUSSION

A. Bulk properties of K^- nuclear bound states

In this subsection we show and discuss results of calculations of 'bulk' properties for K^- nuclear bound states, such as level widths, average nuclear densities and rms radii, and single particle energies. The calculations cover a wide range of binding energies, in order to establish correlations between some of these properties and to study effects due to the nuclear polarization. The empirical values $g_{\sigma K}^{(1)}$ and $g_{\omega K}^{(1)}$ for the RMF $\bar{K}$ coupling constants, as found from a fit to kaonic atom data (third and fourth lines in Table I of Ref. [14]), were used as a starting point for calculations.

A full dynamical calculation was then made for K^- *nuclear* states starting from the static $t\rho$ imaginary potential obtained from the atomic fit with $\mathrm{Im}b_0 = 0.62$ fm from Table I, while entering dynamically in the iteration cycles the resulting nuclear density and the suppression factor f as defined by Eq.(21). This *dynamical* calculation, for the light nuclei ^{12}C and ^{16}O, led to a substantial increase of the calculated binding energy. For example, whereas the static calculation gave $B_{K^-} = 132$ MeV for the $1s$ state in ^{12}C, the dynamical calculation gave $B_{K^-} = 172$ MeV for this same state. In this work, in order to produce different values of binding energies, we focus on a particular way of varying the depth of the real K^--nucleus potential by scaling down successively $g_{\sigma K}$ from its initial value $g^{(1)}_{\sigma K}$ and, once it reaches zero, scaling down $g_{\omega K}$ too from its initial value $g^{(1)}_{\omega K}$ until the K^- $1s$ state became unbound. Obviously, the good *global* fit to the atomic data is inevitably lost once the coupling constants are varied in order to scan over a wide range of binding energies. The reverse procedure of first scaling down $g_{\omega K}$ from its initial value $g^{(1)}_{\omega K}$ to zero, and then reducing $g_{\sigma K}$ from its initial value $g^{(1)}_{\sigma K}$ until the K^- $1s$ state became unbound, gave very similar results except for weak binding where the calculated widths are larger than 100 MeV and hence are outside of our direct interest. Furthermore, in order to scan the region of large values of B_{K^-}, of order 200 MeV, we also scaled up $g_{\sigma K}$ from its initial value $g^{(1)}_{\sigma K}$ while keeping $g_{\omega K} = g^{(1)}_{\omega K}$. In Ref. [30] we have shown that similar results are obtained for different starting values for $g_{\sigma K}$ and $g_{\omega K}$, adjusted to a 'shallow' variety potential [6]. We have also shown there the little sensitivity to the nuclear RMF model version chosen, the linear version L-HS [39] and the nonlinear version NL-SH [40]. Below we discuss some aspects of the sensitivity to the nonlinear version used, particularly for high nuclear densities.

Figure 4 shows calculated widths Γ_{K^-} as function of the binding energy B_{K^-} for $1s$ states in ${}^{12}_{K^-}$C, ${}^{40}_{K^-}$Ca, ${}^{208}_{K^-}$Pb, for the nonlinear NL-SH version [40] of the RMF model. The dotted line shows the static 'nuclear-matter' limit

$$\Gamma_{K^-} \;=\; \frac{f}{1-\frac{B_{K^-}}{m_K}}\;\Gamma^{(0)}_{K^-} \quad , \tag{22}$$

where f is the phase-space suppression factor of Eq. (21) and $\Gamma^{(0)}_{K^-}$ is given by

$$\Gamma^{(0)}_{K^-} \;=\; \frac{4\pi}{\mu_{KN}}\;\mathrm{Im}b_0\;\rho_0 \quad , \tag{23}$$

for the static value $\mathrm{Im}b_0 = 0.62$ fm used in the calculations and for $\rho_0 = 0.16$ fm^{-3}. Eq. (23) holds for a K^- Schroedinger wavefunction which is completely localized within the nuclear central-density ρ_0 region. The additional factor $(1 - B_{K^-}/m_K)^{-1}$ in Eq. (22) follows from using the KG equation rather than the Schroedinger equation. A small correction term of order V_c/m_K was neglected in this factor. It is clearly seen that the dependence of the width of the K^- nuclear state on its binding energy follows the shape of the dotted line for the static nuclear-matter limit of Γ_{K^-}, Eq. (22). This dependence is due primarily to the binding-energy dependence of the suppression factor f which falls off rapidly until $B_{K^-} \sim 100$ MeV, where the dominant $\bar{K}N \to \pi\Sigma$ gets switched off, and then stays rather

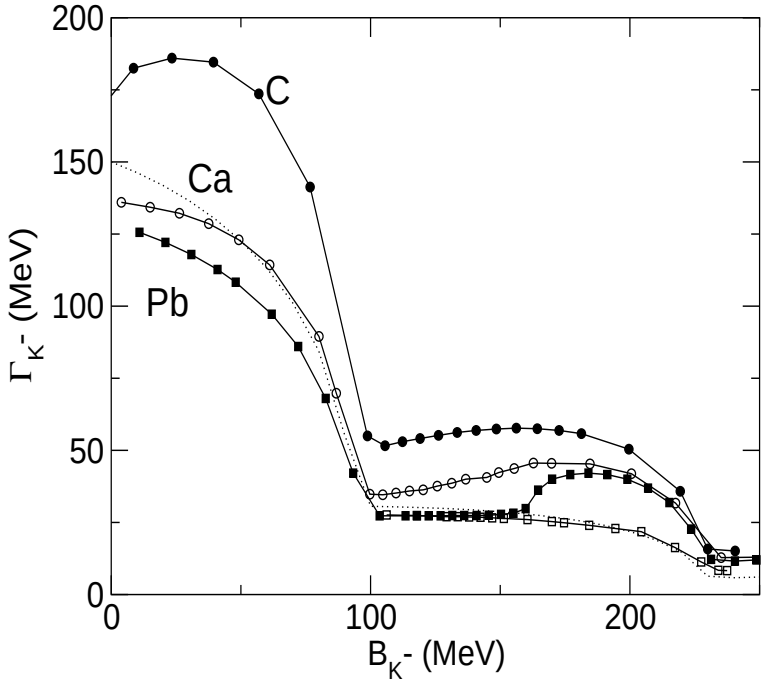

FIG. 4: Dynamically calculated widths of the $1s$ K^--nuclear state in ${}^{12}_{K^-}$C, ${}^{40}_{K^-}$Ca and ${}^{208}_{K^-}$Pb as function of the K^- binding energy, for the NL-SH RMF model [40]. For ${}^{208}_{K^-}$Pb, results using the L-HS RMF model [39] are also shown, by open squares. The dotted line is for a static nuclear-matter calculation with $\rho_0 = 0.16$ fm^{-3}.

flat in the range $B_{K^-} \sim 100 - 200$ MeV where the width is dominated by the two-nucleon absorption modes Eq. (19). The larger values of width for the lighter nuclei are due to the dynamical nature of the RMF calculation, whereby the nuclear density is increased by the polarization effect of the K^- as shown in the next figures. We note that the widths calculated in the range $B_{K^-} \sim 100 - 200$ MeV assume values of about $50 - 60$ MeV for ${}^{12}_{K^-}$C, $35 - 45$ MeV for ${}^{40}_{K^-}$Ca, and about $25 - 30$ MeV for ${}^{208}_{K^-}$Pb in the range $B_{K^-} \sim 100 - 160$ MeV, decreasing gradually with A to the 'nuclear matter' dotted-line value of about 25 MeV. However, as is clearly observed in the figure, for ${}^{208}_{K^-}$Pb beginning at $B_{K^-} \sim 160$ MeV, a strong sensitivity to the nonlinear version of the RMF calculation develops whereby, in the NL-SH version [40] used here, the ^{208}Pb s.p. levels undergo significant crossings, the maximal nuclear density increases substantially, and as a result the nuclear rearrangement energy becomes significantly larger. This does not necessarily affect other bulk properties, such as the average nuclear density discussed below, that do not show a similar sensitivity. For this reason we also demonstrate in Fig. 4 by open squares the results of using the linear version L-HS [39] of the RMF calculation for ${}^{208}_{K^-}$Pb above 100 MeV. The nonlinear and linear versions give practically the same results below 160 MeV, and we note assuredly that the behavior of the calculated width as function of the binding energy for the linear version follows closely the 'nuclear matter' dotted line without any interruption around 160 MeV. The compressibility of the nucleus for linear versions is about twice that produced by nonlinear versions which are

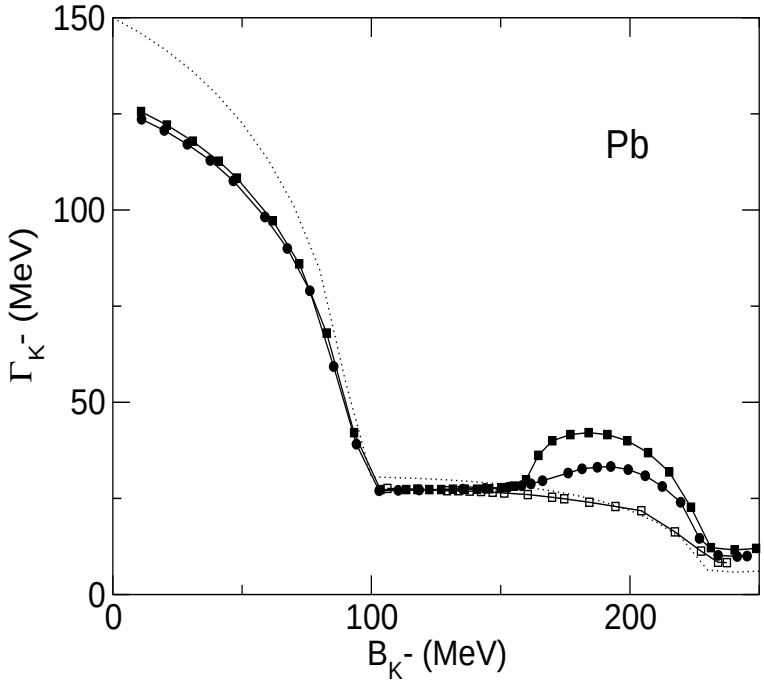

FIG. 5: Dynamically calculated widths of the $1s$ K^--nuclear state in ${}^{208}_{K^-}$Pb as function of the K^- binding energy, for the nonlinear RMF models NL-SH [40] (solid squares) and NL-TM1 [46] (solid circles), and for the linear model L-HS [39] (open squares). The dotted line is for a static nuclear-matter calculation with $\rho_0 = 0.16$ fm^{-3}.

more realistic in this respect, and hence it is more difficult to polarize the nucleus within the linear version.

In order to explore further the sensitivity to the nonlinear version of the RMF calculation, we show in Fig. 5 the calculated widths for ${}^{208}_{K^-}$Pb using in addition to the NL-SH version employed above [40] also the NL-TM1 version due to Sugahara and Toki [46]. The results of using the linear L-HS version [39] are also shown for $B_{K^-} > 100$ MeV, as well as the dotted line for the static muclear-matter calculation specified above. The two nonlinear versions agree with each other very closely below 160 MeV but depart from each other above, with each giving rise to enhanced values of the width. The width evaluated using the NL-TM1 version appears to behave considerably more regularly than the NL-SH version . We note that similar calculations using the NL1 version, which was used in Ref. [14], completely break down for the high nuclear densities encountered in this kinematical region. In contrast, the linear version L-HS [39], with a considerably higher value of nuclear compressibility, does not give rise to any enhancement of the calculated width and it practically coincides with the results of the nuclear-matter static calculation. Another comment is that in the region below 100 MeV, the static nuclear-matter calculation produces higher values of width than any of the RMF versions, since it assumes a perfect overlap of the K^- wavefunction with the central-density region.

To conclude the estimate of K^- widths we comment that replacing ρ by ρ^2 for the density dependence of the

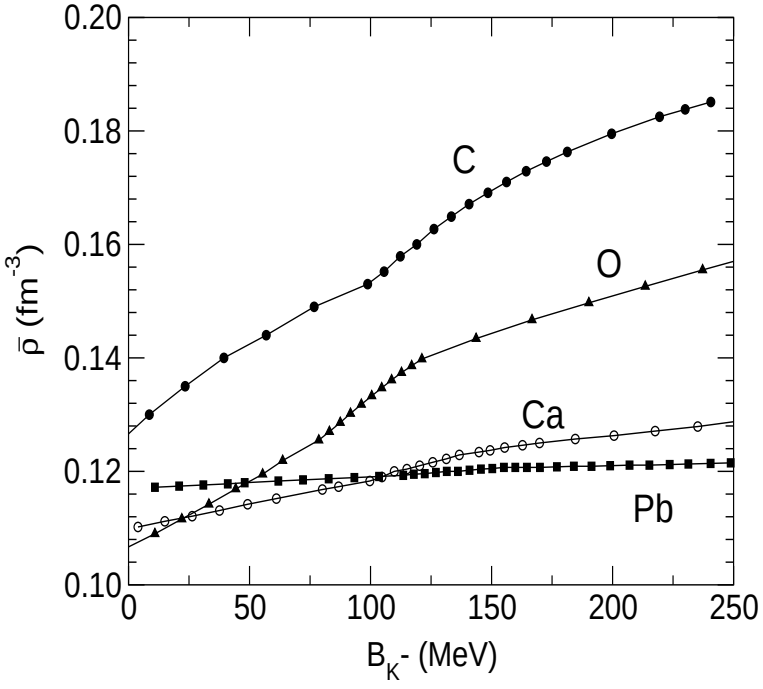

FIG. 6: Calculated average nuclear density $\bar{\rho}$ for ${}_{K^-}^{12}$C, ${}_{K^-}^{16}$O, ${}_{K^-}^{40}$Ca and ${}_{K^-}^{208}$Pb as function of the $1s$ K^- binding energy, for the same nonlinear RMF model as in Fig. 4.

non-pionic decay modes Eq. (19) is estimated to increase the above values of the width by $10-15$ MeV. This estimate follows, again, from the increase of nuclear density with B_{K^-} noticed above. Switching on the $\pi\Lambda$ decay mode would increase further this estimate by $5-10$ MeV in the range $B_{K^-} \sim 100-180$ MeV. We therefore expect that the estimate $\Gamma_{K^-} = 50 \pm 10$ MeV in the range $B_{K^-} \sim 100-200$ MeV provides a reasonable lower bound on the width expected for light and medium-weight nuclei in any realistic calculation.

The next four figures exhibit various nuclear properties, calculated dynamically, for nuclei containing a K^- nuclear $1s$ state. Figure 6 shows the calculated average nuclear density $\bar{\rho} = \frac{1}{A}\int \rho^2 d\mathbf{r}$ as a function of B_{K^-} for the same K^- nuclear $1s$ states as in Fig. 4 and for $1s$ states in ${}_{K^-}^{16}$O which is studied below. The average nuclear density $\bar{\rho}$ increases substantially in the light K^- nuclei, for the binding-energy range shown here, to values about 50% higher than for these nuclei in the absence of the K^- meson. The increase of the central nuclear densities is even bigger, as demonstrated in the next two figures, but is confined to a small region of order 1 fm from the origin. These features point out to a significant polarization of the nuclear core by the $1s$ K^-, particularly in light nuclei.

Figure 7 shows calculated nuclear densities of ${}_{K^-}^{12}$C for several values of the $1s$ K^- binding energies. The purely nuclear density, in absence of the K^- meson, is given by the dashed curve. The maximal value of the nuclear density is increased by up to 75% in the range of binding energies spanned in the figure, and the enhancement is close to uniform over the central 1 fm, decreasing gradually to zero by $r = 2$ fm which already marks the nuclear surface. In

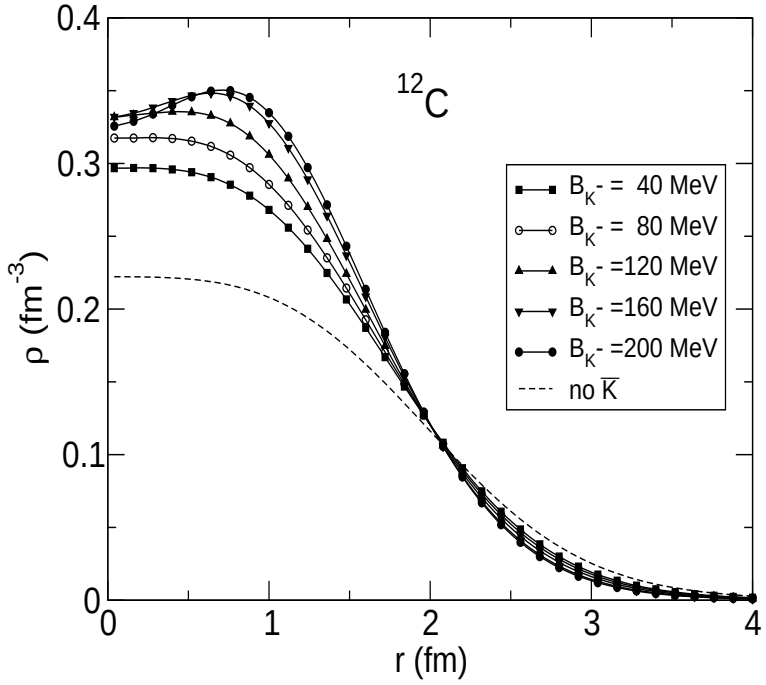

FIG. 7: Calculated nuclear density ρ of ${}_{K^-}{}^{12}$C for several $1s$ K^- nuclear states with specified B_{K^-} values, using the nonlinear RMF model NL-SH [40] as in Fig. 4. The dashed curve stands for the ^{12}C density in the absence of the K^- meson.

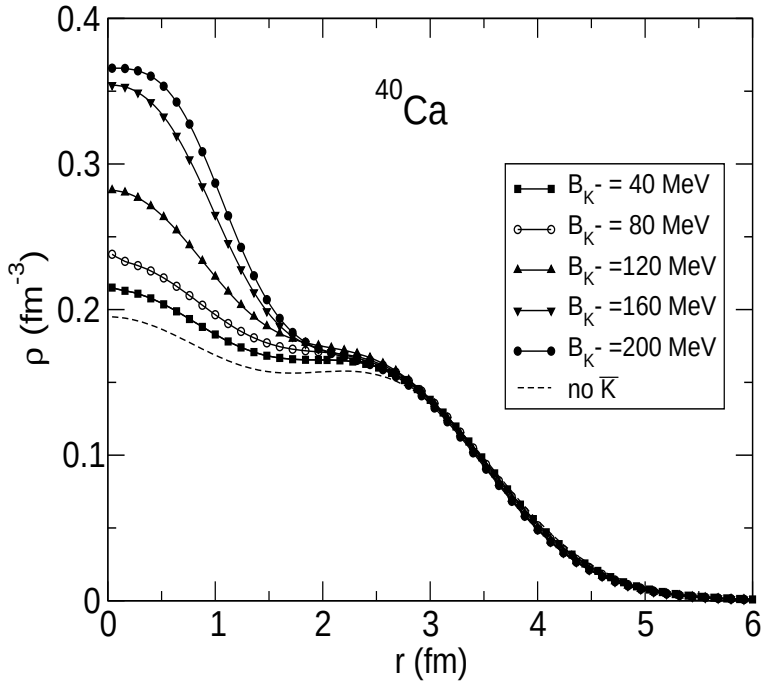

FIG. 8: Calculated nuclear density ρ of ${}_{K^-}{}^{40}$Ca for several $1s$ K^- nuclear states with specified B_{K^-} values, using the nonlinear RMF model NL-SH [40] as in Fig. 4. The dashed curve stands for the ^{40}Ca density in the absence of the K^- meson.

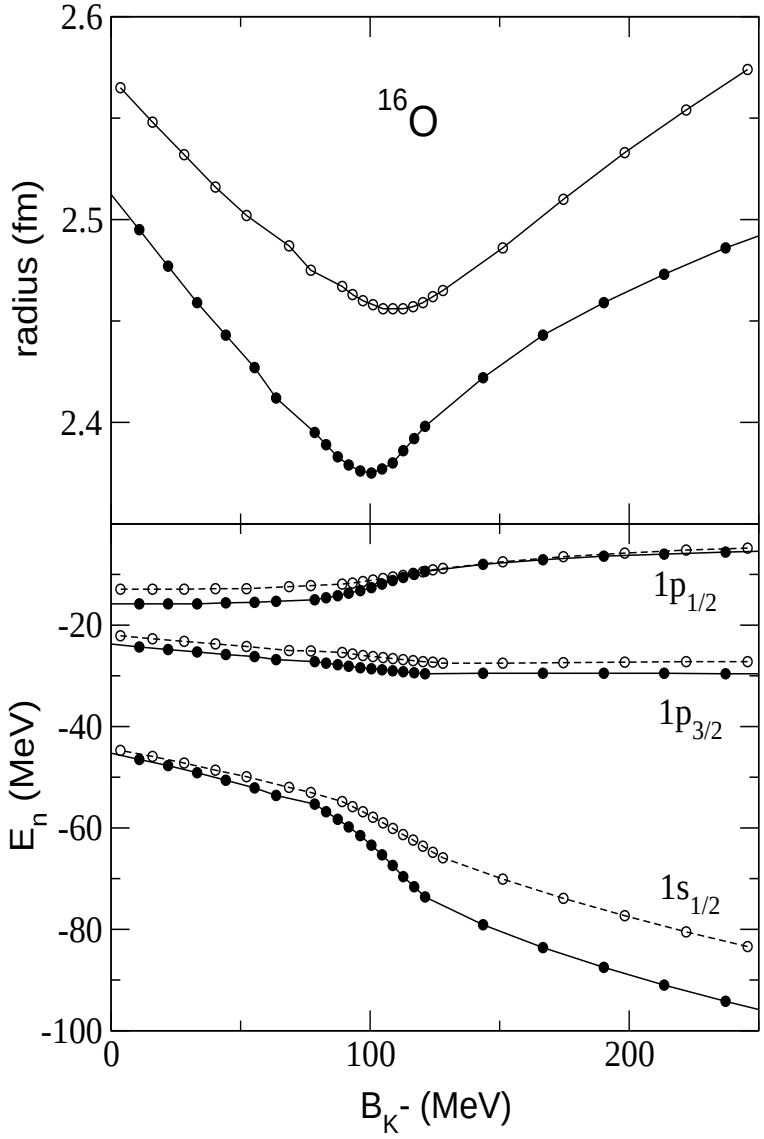

FIG. 9: Nuclear rms radius and neutron single-particle energies for ${}^{16}_{K^-}$O as function of the $1s$ K^- binding energy, for the linear RMF model L-HS [39] (open circles) and the nonlinear RMF model NL-SH [40] (solid circles) used in Fig. 4.

this fairly small nucleus, the density is enhanced over a substantial portion of the nucleus. This is different than in heavier nuclei, as shown in Fig. 8 for the medium-weight ${}^{40}_{K^-}$Ca. Here, the enhancement of the maximal density (at the center of the nucleus) reaches almost a factor of two, but it subsides almost completely by $r = 2$ fm which is still well within the nuclear volume (the nuclear radius of ^{40}Ca is about 3.5 fm). This localization of the nuclear-density enhancement is due to the localized $1s$ K^- density. As a result, the *average* nuclear density of ${}^{40}_{K^-}$Ca shown in Fig. 6 is only weakly enhanced as function of B_{K^-}. In heavier nuclei such as ^{208}Pb, the localization of the $1s$ K^- density is as pronounced and the resultant nuclear density is enhanced by more than a factor of two over a small portion of the nucleus, confined again to the region $r \lesssim 2$ fm.

The upper and lower panels of Fig. 9 show the calculated nuclear rms radius and the $1s$ and $1p$ neutron single-particle energies E_n, respectively, for ${}^{16}_{K^-}$O as a function of B_{K^-}, for two versions of the RMF calculation, the linear model L-HS [39] (open circles) and the nonlinear model NL-SH [40] (solid circles). The figure shows clearly that the polarization effect of the $1s$ K^- bound state on the $1s$ nuclear bound state is particularly strong. The differences between the linear and nonlinear models reflect the different nuclear compressibility and the somewhat different nuclear sizes obtained in the two models. It is interesting to note that the increase in the nuclear rms radius of ${}^{16}_{K^-}$O for large values of B_{K^-} is the result of the reduced binding energy of the $1p_{1/2}$ state, due to the increased spin-orbit term. Note also that as B_{K^-} approaches zero we do *not* recover the values inherent in static calculations for the various nuclear entities in Fig. 6 and Fig. 9, because at $B_{K^-}=0$ both $\mathrm{Re}V^{\bar{K}}_{\mathrm{opt}}$ and $\mathrm{Im}V^{\bar{K}}_{\mathrm{opt}}$ are still far from assuming zero values.

The polarization effects noted here in both Fig. 6 and Fig. 9 are somewhat larger than in Fig. 2 and Fig. 3 of our Letter publication [30]. This is due to the energy dependent suppressive factor in front of the vector potential in Eq. (15) which was disregarded there and which requires stronger couplings of the $\bar{K}$ in order to reproduce the same value of B_{K^-} as before. However, the effect of this suppressive factor on the calculated widths is minor as long as the width is plotted as function of the binding energy, as done here in Fig. 4 and in Fig. 1 of Ref. [30], mainly because the dominant factor in the calculation of the width is the phase-space suppression factor f which is directly determined by B_{K^-}. A welcome by-product of the present revision is that the 'deep' potential fitted in section II to the K^- atomic data produces K^- nuclear bound states in light nuclei in the range of interest, $B_{K^-}\sim 100-200$ MeV, where several claims for bound states have recently been made [26, 27, 28, 29]. This is discussed in the next subsection.

B. Selected examples

The discussion in this subsection is related to the FINUDA experiment [29] at DAΦNE, Frascati, which recently suggested evidence for a K^-pp bound state produced in K^- absorption at rest on unresolved combination of ^{6}Li, ^{7}Li and ^{12}C targets. The experiment looked for back-to-back Λp pairs, assigned to the strong decay $K^-pp\to\Lambda p$ which is a special case of Eq. (19). In addition to observing Λp pairs which correspond kinematically to K^-pp essentially at rest, a peak in the invariant mass of Λp pairs was found that corresponds in the interpretation of Ref. [29] to a K^-pp cluster bound by $B_{K^-pp}=115\pm 6\pm 4$ MeV with a decay width $\Gamma=67\pm 14\pm 3$ MeV. We comment that the mere observation of back-to-back Λp pairs from the decay of a K^-pp cluster does not mean that this cluster is self-bound in the nucleus, in as much as the observation of back-to-back np pairs in the weak hypernuclear decay of Λ hypernuclei does not mean that Λp clusters are self-bound in the nuclear medium. Since the $\bar{K}$-nucleus potential is at least as strong as the Λ-nucleus potential, the most natural expectation is for $\bar{K}$-nuclear bound states similar to the well

TABLE II: Binding energy B_{K^-} calculated statically and dynamically, nuclear rearrangement energy $R^{\rm dyn}_{\rm nucl}$ and width Γ_{K^-} calculated dynamically, for the $1s$ K^- - nuclear bound state in ${}^{6}_{K^-}$Li, ${}^{12}_{K^-}$C, ${}^{16}_{K^-}$O, ${}^{40}_{K^-}$Ca and ${}^{208}_{K^-}$Pb, using coupling-constant ratios $\alpha_\sigma = g_{\sigma K}/g^{(1)}_{\sigma K} = 0$ and $\alpha_\omega = g_{\omega K}/g^{(1)}_{\omega K} = 0.95$.

nucleus	$B^{\rm stat}_{K^-}$ (MeV)	$B^{\rm dyn}_{K^-}$ (MeV)	$R^{\rm dyn}_{\rm nucl}$ (MeV)	$\Gamma^{\rm dyn}_{K^-}$ (MeV)
^{6}Li	28.1	35.6	17.0	229.1
^{12}C	71.6	88.7	10.6	94.9
^{16}O	66.0	72.6	7.6	100.4
^{40}Ca	88.7	93.3	4.2	51.6
^{208}Pb	107.3	108.5	1.3	27.3

accepted spectra of Λ-nuclear bound states over the periodic table beginning with $A = 3$. The interpretation of the FINUDA events in terms of a K^-pp bound state requires that its binding energy is independent of the nuclear target off which back-to-back Λp pairs are emitted. At present the data do not allow to extract a statistically significant signal from individual targets used in the experiment. Since the constitution of targets in the FINUDA experiment favors ^{12}C, we will assume for the sake of argument that this observed peak corresponds to a $1s$ or a $1p$ K^- bound state in ^{12}C, or perhaps in ^{11}C or ^{11}B corresponding to production by the (K^-, n) or (K^-, p) reactions respectively. The consequences of this working hypothesis for the other targets will then be considered. Subtracting $B_{pp} = 27.2$ MeV from the binding energy 115 MeV assigned in Ref. [29] to the K^-pp-cluster binding, the relevant K^- binding energy is $B_{K^-} \sim 88$ MeV. Regarding the width assigned by the FINUDA experiment to the bound-state signal, it could partly arise from Fermi-motion broadening which in the Fermi gas model yields the following contribution:

$$\frac{\Gamma_F}{2} = \sqrt{< (\frac{p^2}{m_N})^{\,2} > - < \frac{p^2}{m_N} >^{\,2}} = \frac{2}{5}\sqrt{\frac{3}{7}}\frac{p_F^2}{m_N} = 20.3 \text{ MeV} \quad (p_F = 270 \text{ MeV/c}) \ . \tag{24}$$

This will reduce (quadratically) the assigned width of about 67 MeV down to 53 MeV. A rather broad distribution of back-to-back Λp events may also arise without invoking a bound state of any sort, due to the combination of Fermi motion of the initial pp pair and the nuclear final-state interactions of the emitted Λp pair, as shown by Magas et al. [47] after submission of the present work for publication.

In Table II we show results of static and dynamical calculations for $1s$ states in ${}^{6}_{K^-}$Li, ${}^{12}_{K^-}$C, ${}^{16}_{K^-}$O, ${}^{40}_{K^-}$Ca and ${}^{208}_{K^-}$Pb, choosing the coupling constants $g_{\sigma K}$ and $g_{\omega K}$ such that $B_{K^-} \sim 88$ MeV for the $1s$ ground state of ${}^{12}_{K^-}$C in the dynamical calculation. These coupling constants are not close to those required to produce the K^- atoms best fit, and the K^- potential determined here is considerably weaker than the potential of type DD or F in Fig. 1. A comparison between the very different binding energies calculated for ${}^{6}_{K^-}$Li and ${}^{12}_{K^-}$C leads to the conclusion that the peak observed in the FINUDA experiment cannot result from *both* Li and C. The relatively weak binding calculated

for ${}^{6}_{K^-}$Li implies, in agreement with Fig. 4 for other nuclei, a huge value of over 200 MeV for the width. The width of the ${}^{12}_{K^-}$C $1s$ state is smaller, $\Gamma = 95$ MeV, but is larger than the width of the observed peak. These conclusions do not change upon slightly increasing $g_{\omega K}$ from 0.95 to 0.985, so that $B_{K^-} \sim 88$ MeV holds for ${}^{11}_{K^-}$C instead of for ${}^{12}_{K^-}$C. We then find $B_{K^-} = 88.6(95.9)$ MeV and $\Gamma_{K^-} = 96.9(66.5)$ MeV for ${}^{11(12)}_{K^-}$C, while ${}^{6}_{K^-}$Li is considerably less bound.

We note in Table II the relatively strong variation of the calculated binding energies between ${}^{12}_{K^-}$C and ${}^{16}_{K^-}$O which is due to the difference between the underlying nuclear density input for these nuclei in the static RMF calculation. Choosing only *one* of these nuclei for the mass-number A systematics, the results of the table may be summarized as follows:

- The K^- binding energy increases monotonically as a function of A. However, without the Coulomb potential V_c it is almost constant from ^{12}C on due to saturation.
- The width decreases monotonically with A, which is a corollary of the $\Gamma(B_{K^-})$ dependence in Fig. 4.
- Except for ${}^{6}_{K^-}$Li where the binding energy is relatively small, the difference between the binding energies calculated dynamically and statically is substantial in light nuclei, decreasing monotonically with A, and may be neglected only for very heavy nuclei.
- The dynamical effect is very strong for ${}^{12}_{K^-}$C where the increase in the dynamically calculated B_{K^-} is 17 MeV with respect to the static calculation. This increase gets larger with B_{K^-}, as demonstrated in the previous subsection for $\alpha_\sigma = \alpha_\omega = 1$ where it amounts to 40 MeV.
- The nuclear rearrangement energy, defined here as $R^{\rm dyn}_{\rm nucl} = B^{\rm s.p.}_{K^-} - B_{K^-}$ in the dynamical calculation, decreases monotonically with A. For a given value of A, however (but not demonstrated here), $R^{\rm dyn}_{\rm nucl}$ increases with B_{K^-}.

Except for ${}^{6}_{K^-}$Li, all the K^- nuclei demonstrated in Table II have additional bound states for the specified coupling constants. Thus, both ${}^{12}_{K^-}$C and ${}^{16}_{K^-}$O have bound $1p$ states, with $B^{\rm dyn}_{K^-} = 16.6,\ 30.6$ MeV, respectively, but with very large widths: $\Gamma^{\rm dyn}_{K^-} = 158,\ 123$ MeV, respectively. We therefore have an unfavorable situation of overlapping $1s$ and $1p$ levels.

In Table III, we compare between dynamical calculations for ${}^{6}_{K^-}$Li and ${}^{12}_{K^-}$C, requiring that $B_{K^-} \sim 88$ MeV now holds for the $1p$ instead of the $1s$ state in ${}^{12}_{K^-}$C. This requirement is motivated by the recent calculations of Yamagata et al. [48] according to which the $1p$ production cross section in (K^-, N) reactions is higher than for the $1s$ state. The requirement $B_{K^-} \sim 88$ MeV for the $1p$ state in ${}^{12}_{K^-}$C is satisfied using kaon coupling constants only slightly different than those found optimal for the K^- atomic fit of Ref. [14]. The width of this $1p$ state, 89 MeV, is close to the value 95 MeV listed in Table II for the $1s$ state constrained to the same binding energy. The $1s$ states calculated in this case

TABLE III: Binding energy B_{K^-} and width Γ_{K^-} calculated statically and dynamically for the K^- - nuclear $1s$ and $1p$ states in ${}^{6}_{K^-}$Li and ${}^{12}_{K^-}$C, using $\alpha_\sigma = 1.1$ and $\alpha_\omega = 1.0$.

nucleus	nl	$B^{\rm stat}_{K^-}$ (MeV)	$\Gamma^{\rm stat}_{K^-}$ (MeV)	$B^{\rm dyn}_{K^-}$ (MeV)	$\Gamma^{\rm dyn}_{K^-}$ (MeV)
^{6}Li	$1s$	75.1	79.0	146.5	74.5
	$1p$	4.1	70.7	7.4	184.4
^{12}C	$1s$	137.6	34.5	181.3	55.7
	$1p$	67.5	97.8	88.6	89.3

for the two nuclei are narrower than the respective $1p$ states, simply because their widths are suppressed stronger by the phase-space suppression factor f. The increase in B_{K^-} for these deeply bound $1s$ states provided by going from the static calculation to the dynamical one is very substantial, with exceptionally large value of 71 MeV due to the strong polarization that the ^{6}Li nucleus undergoes due to a deeply bound K^-. We note that for very shallow bound states, as demonstrated here for the ${}^{6}_{K^-}$Li $1p$ state and as will be shown in Fig. 10 below for the ${}^{12}_{K^-}$C $1s$ state, there is little difference between the static and the dynamical calculations for B_{K^-}. In contrast, the width Γ_{K^-} is very strongly enhanced in ${}^{6}_{K^-}$Li owing to the increase of the nuclear density provided by the dynamical calculation, from 71 MeV in the static calculation to 184 MeV in the dynamical calculation for the $1p$ state. Although the width of the $1s$ state hardly changes, it would have decreased by roughly factor of two due to the phase-space suppression factor f if the increase of the nuclear density did not offset this decrease.

A comparison between the statically calculated (open circles) and the dynamically calculated (solid circles) B_{K^-} and Γ_{K^-} for the $1s$ state in ${}^{12}_{K^-}$C is shown in Fig. 10 as a function of the coupling-constant strenghts. It is clear that for $B_{K^-} > 25$ MeV the dynamical calculation gives higher binding than the static calculation does, with the binding-energy gain increasing monotonically with B_{K^-}, and this effect becomes important for $B_{K^-} > 50$ MeV. The effect on Γ_{K^-} is more intricate: the dynamically calculated width is larger than the width calculated statically, except in the region around $B_{K^-} \sim 100$ MeV where the kinematical phase-space suppression factor f of Eq. (21) decreases rapidly. In this region, the dynamically calculated Γ_{K^-} corresponds to binding energy B_{K^-} which is associated with a considerably more suppressed value of f than in the static calculation, and this effect wins over the width gained by the increased nuclear density. We note that the width calculated dynamically for the $1s$ nuclear state in ${}^{12}_{K^-}$C does not fall below 50 MeV for the range of variation shown, whereas the corresponding limiting value of the statically calculated width is about 35 MeV. Another feature shown in Fig. 10 concerns the effect of the imaginary potential on the binding energy: the dynamically calculated binding energy B_{K^-} when Im$V_{\rm opt}$ is switched off is shown by the dotted line. It is clear that the absorptive potential Im$V_{\rm opt}$ acts *repulsively* and its inclusion leads to less binding, particularly at low

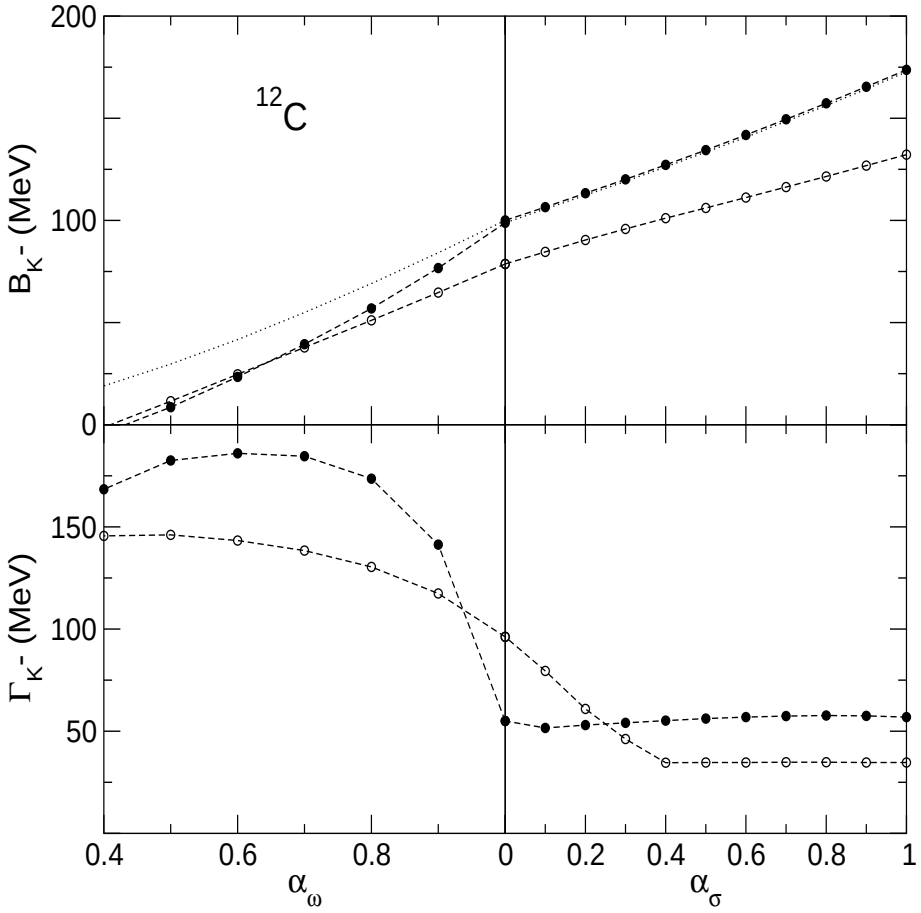

FIG. 10: $1s$ K^- binding energy and width in ${}_{K^-}^{12}$C calculated statically (open circles) and dynamically (solid circles) for the nonlinear RMF model NL-SH [40] as function of the ωK and σK coupling strengths: α_ω is varied in the left panels as indicated, with $\alpha_\sigma = 0$, and α_σ is varied in the right panels as indicated, with $\alpha_\omega = 1$. The dotted line shows the calculated binding energy when the absorptive K^- potential is switched off in the dynamical calculation.

binding energies. In fact, without Im$V_{\rm opt}$ we would *always* have $B_{K^-}^{\rm dyn} > B_{K^-}^{\rm stat}$. The repulsive effect of Im$V_{\rm opt}$ gets weaker with B_{K^-}, along with the action of the suppression factor f, and beginning with $B_{K^-} \sim 100$ MeV it hardly matters for the calculation of B_{K^-} whether or not Im$V_{\rm opt}$ is included.

Finally, we comment on the outcome of making $g_{\omega K}$ density dependent,

$$g_{\omega K}(\rho) \;=\; \frac{g_{\omega K}(0)}{1 \;-\; 0.046\sigma\rho} \quad , \tag{25}$$

similar to the density dependence on the rhs in Eq. (5), which according to Ref. [15] might simulate partial restoration of chiral symmetry in dense medium. The starting parameters for the static calculation corresponded to a 'shallow' $\bar{K}$-nucleus potential of depths about 60 MeV for both real and imaginary parts. For this choice ${}_{K^-}^{12}$C and ${}_{K^-}^{16}$O have just one bound state ($1s$) each, with binding energy $B_{K^-}^{\rm dyn} = 5.3,\ 22.8$ MeV, respectively. The introduction of the density dependence Eq. (25) within a dynamical calculation increases the binding energy to about $70 - 80$ MeV.

However, the width of these states is large, close to 100 MeV. We conclude that although this ansatz for density dependence did not improve the fit to kaonic atoms data where the need to introduce phenomenological density dependence appears at low densities, its role in the higher nuclear density regime [13] and for generating nuclear $\bar{K}$ bound states cannot be ruled out at present.

V. SUMMARY

In this work we re-analyzed the data on strong-interaction effects in K^- atoms across the periodic table in order to study the density dependence of $V_{\rm opt}^{\bar{K}}$ and its extrapolation into nuclear-matter densities. A departure from the $t_{\rm eff}\rho$ dependence was found at the 20% range of nuclear-matter density ρ_0. Partial restoration of chiral symmetry, such as discussed in low energy pion-nuclear physics, was found to be ineffective at this low-density regime, but its role at higher densities cannot be ruled out. A smooth extrapolation into the nuclear interior gave a *deep* $\bar{K}$ nuclear potential $V_{\rm opt}^{\bar{K}}$ which would allow the existence of $\bar{K}$ nuclear bound states even for a static calculation. We then extended the purely nuclear RMF model by coupling the $\bar{K}$ *dynamically* to the nucleus. Negligible polarization effects were found for *atomic* states, which confirms the optical-potential phenomenology of kaonic atoms in general, and as a valid starting point for the present study in particular. Binding energies and widths of $\bar{K}$ *nuclear* bound states were then calculated across the periodic table with the aim of placing lower limits on the widths expected for binding energies in the range of $100-200$ MeV. Substantial polarization of the nucleus was found in light nuclei such as ^{12}C and ^{16}O for deeply bound $\bar{K}$ nuclear states, resulting in locally increased nuclear densities up to about $2\rho_0$. An almost universal shape was found for the dependence of the $\bar{K}$ width on its binding energy. The widths are primarily suppressed by the reduced phase-space for absorption of $\bar{K}$, and are enhanced by the increased density of the polarized nucleus. The present results already provide useful guidance for the interpretation of the recent FINUDA experimental results [29] by presenting some calculated dependence on the atomic mass number A and placing a lower limit $\Gamma_{\bar{K}} \sim 50 \pm 10$ MeV on $\bar{K}$ states bound in the range $B_{\bar{K}} \sim 100-200$ MeV. Our calculated widths for a K^- $1s$ or $1p$ bound state in ^{12}C, in the kinematical region of the FINUDA signal, are about 90 MeV which is somewhat larger than the reported width. We noted that a $1p$ bound state in ^{12}C, rather than $1s$ bound state, is compatible with the 'deep' type of K^--nucleus potential fitted to the atomic data and perhaps also with deeply bound K^- $1s$ states in the range $B_K \sim 150-200$ MeV for lighter nuclear targets such as ^{4}He [26, 27]. We have argued that if the FINUDA observed signal corresponds to a $\bar{K}$ bound state in ^{12}C, then it is unlikely to arise in Li targets, thus emphasizing the need to get statistically significant data from separate nuclear targets. For lighter nuclear targets, where the RMF approach becomes unreliable but where nuclear polarization effects are found much larger using few-body calculational methods [34], we anticipate larger widths than 50 MeV for $\bar{K}$ deeply bound states in the range $B_K \sim 100-200$ MeV.

Acknowledgments

This work was supported in part by the GA AVCR grant A100480617 and by the Israel Science Foundation grant 757/05.

---

[1] R.H. Dalitz, T.C. Wong, G. Rajasekaran, Phys. Rev. 153 (1967) 1617.

[2] A.D. Martin, Phys. Lett. 65B (1976) 346.

[3] T. Waas, M. Rho, W. Weise, Nucl. Phys. A 617 (1997) 449; and references therein.

[4] T. Waas, N. Kaiser, W. Weise, Phys. Lett. B 379 (1996) 34.

[5] J. Schaffner-Bielich, V. Koch, M. Effenberger, Nucl. Phys. A 669 (2000) 153.

[6] A. Ramos, E. Oset, Nucl. Phys. A 671 (2000) 481.

[7] A. Cieplý, E. Friedman, A. Gal, J. Mareš, Nucl. Phys. A 696 (2001) 173.

[8] E. Friedman, A. Gal, C.J. Batty, Phys. Lett. B 308 (1993) 6.

[9] E. Friedman, A. Gal, C.J. Batty, Nucl. Phys. A 579 (1994) 518.

[10] C.J. Batty, E. Friedman, A. Gal, Phys. Rep. 287 (1997) 385.

[11] J. Schaffner, A. Gal, I.N. Mishustin, H. Stöcker, W. Greiner, Phys. Lett. B 334 (1994) 268.

[12] J. Schaffner, I.N. Mishustin, Phys. Rev. C 53 (1996) 1416.

[13] G.E. Brown, M. Rho, Nucl. Phys. A 596 (1996) 503.

[14] E. Friedman, A. Gal, J. Mareš, A. Cieplý, Phys. Rev. C 60 (1999) 024314.

[15] W. Weise, Nucl. Phys. A 690 (2001) 98c.

[16] J. Gasser, H. Leutwyler, M.E. Sainio, Phys. Lett. B 253 (1991) 252.

[17] E. Friedman, Phys. Lett. B 524 (2002) 87.

[18] E. Friedman, Nucl. Phys. A 710 (2002) 117.

[19] E.E. Kolomeitsev, N. Kaiser, W. Weise, Phys. Rev. Lett. 90 (2003) 092501.

[20] E. Friedman, A. Gal, Nucl. Phys. A 724 (2003) 143.

[21] E. Friedman, A. Gal, Phys. Lett. B 578 (2004) 85.

[22] K. Suzuki, M. Fujita, H. Geissel, H. Gilg, A. Gillitzer, R.S. Hayano, S. Hirenzaki, K. Itahashi, M. Iwasaki, P. Kienle, M. Matos, G. Münzenberg, T. Ohtsubo, M. Sato, M. Shindo, T. Suzuki, H. Weick, M. Winkler, T. Yamazaki, T. Yoneyama, Phys. Rev. Lett. 92 (2004) 072302.

[23] E. Friedman, M. Bauer, J. Breitschopf, H. Clement, H. Denz, E. Doroshkevich, A. Erhardt, G.J. Hofman, R. Meier, G.J. Wagner, G. Yaari, Phys. Rev. Lett. 93 (2004) 122302.

[24] E. Friedman, M. Bauer, J. Breitschopf, H. Clement, H. Denz, E. Doroshkevich, A. Erhardt, G.J. Hofman, S. Kritchman, R. Meier, G.J. Wagner, G. Yaari, Phys. Rev. C 72 (2005) 034609.

[25] C.J. Batty, E. Friedman, A. Gal, Nucl. Phys. A 592 (1995) 487.

[26] T. Suzuki, H. Bhang, G. Franklin, K. Gomikawa, R.S. Hayano, T. Hayashi, K. Ishikawa, S. Ishimoto, K. Itahashi, M. Iwasaki, T. Katayama, Y. Kondo, Y. Matsuda, T. Nakamura, S. Okada, H. Outa, B. Quinn, M. Sato, M. Shindo, H. So, P. Strasser, T. Sugimoto, K. Suzuki, S. Suzuki, D. Tomono, A.M. Vinodkumar, E. Widmann, T. Yamazaki, T. Yoneyama, Phys. Lett. B 597 (2004) 263.

[27] T. Suzuki, H. Bhang, G. Franklin, K. Gomikawa, R.S. Hayano, T. Hayashi, K. Ishikawa, S. Ishimoto, K. Itahashi, M. Iwasaki, T. Katayama, Y. Kondo, Y. Matsuda, T. Nakamura, S. Okada, H. Outa, B. Quinn, M. Sato, M. Shindo, H. So, P. Strasser, T. Sugimoto, K. Suzuki, S. Suzuki, D. Tomono, A.M. Vinodkumar, E. Widmann, T. Yamazaki, T. Yoneyama, Nucl. Phys. A 754 (2005) 375c.

[28] T. Kishimoto, T. Hayakawa, S. Ajimura, S. Minami, A. Sakaguchi, Y. Shimizu, R.E. Chrien, M. May, P. Pile, A. Rusek, R. Sutter, H. Noumi, H. Tamura, M. Ukai, Y. Miura, K. Tanida, Nucl. Phys. A 754 (2005) 383c.

[29] M. Agnello, G. Beer, L. Benussi, M. Bertani, S. Bianco, E. Botta, T. Bressani, L. Busso, D. Calvo, P. Camerini, P. Cerello, B. Dalena, F. De Mori, G. D'Erasmo, D. Di Santo, F.L. Fabbri, D. Faso, A. Feliciello, A. Filippi, V. Filippini, E.M. Fiore, H. Fujioka, P. Gianotti, N. Grion, V. Lucherini, S. Marcello, T. Maruta, N. Mirfakhrai, O. Morra, T. Nagae, A. Olin, H. Outa, E. Pace, M. Palomba, A. Pantaleo, A. Panzarasa, V. Paticchio, S. Piano, F. Pompili, R. Rui, G. Simonetti, H. So, S. Tomassini, A. Toyoda, R. Wheadon, A. Zenoni, Phys. Rev. Lett. 94 (2005) 212303.

[30] J. Mareš, E. Friedman, A. Gal, Phys. Lett. B 606 (2005) 295.

[31] W. Weise, contribution to the International Conference on Exotic Atoms, Vienna, February 2005, arXiv:nucl-th/0507058.

[32] G.E. Brown, C.-H. Lee, M. Rho, V. Thorsson, Nucl. Phys. A 567 (1994) 937.

[33] Y. Akaishi, T. Yamazaki, Phys. Rev. C 65 (2002) 044005.

[34] Y. Akaishi, A. Doté, T. Yamazaki, Phys. Lett. B 613 (2005) 140.

[35] E. Friedman, A. Gal, J. Mareš, Nucl. Phys. A 761 (2005) 283.

[36] T. Bürvenich, I.N. Mishustin, L.M. Satarov, J.A. Maruhn, H. Stöcker, W. Greiner, Phys. Lett. B 542 (2002) 261.

[37] I.N. Mishustin, L.M. Satarov, T.J. Bürvenich, H. Stöcker, W. Greiner, Phys. Rev. C 71 (2005) 035201.

[38] X.H. Zhong, G.X. Peng, L. Li, P.Z. Ning, *$\bar{K}$-Nuclear Bound States in RMF Theory*, arXiv:nucl-th/0508031.

[39] C.J. Horowitz, B.D. Serot, Nucl. Phys. A 368 (1981) 503.

[40] M.M. Sharma, M.A. Nagarajan, P. Ring, Phys. Lett. B 312 (1993) 377.

[41] C. Vander Velde-Wilquet, J. Sacton, J.H. Wickens, D.N. Tovee, D.H. Davis, Nuovo Cimento A 39 (1977) 538.

[42] D.S. Koltun in *Meson-Nuclear Physics 1979*, ed. E.V. Hungerford III, AIP Conf. Proc. 54 (AIP, New York, 1979) 87.

[43] J. Mareš, E. Friedman, A. Gal, B.K. Jennings, Nucl. Phys. A 594 (1995) 311.

[44] H. Noumi, P.K. Saha, D. Abe, S. Ajimura, K. Aoki, H.C. Bhang, T. Endo, Y. Fujii, T. Fukuda, H.C. Guo, K. Imai, O. Hashimoto, H. Hotchi, E.H. Kim, J.H. Kim, T. Kishimoto, A. Krutenkova, K. Maeda, T. Nagae, M. Nakamura, H. Outa, M. Sekimoto, T. Saito, A. Sakaguchi, Y. Sato, R. Sawafta, Y. Shimizu, T. Takahashi, L. Tang, H. Tamura, K. Tanida, T. Watanabe, H.H. Xia, S.H. Zhou, L.H. Zhu, X.F. Zhu, Phys. Rev. Lett. 89 (2002) 072301; ibid. 90 (2003) 049902(E).

[45] P.K. Saha, H. Noumi, D. Abe, S. Ajimura, K. Aoki, H.C. Bhang, K. Dobashi, T. Endo, Y. Fujii, T. Fukuda, H.C. Guo, O. Hashimoto, H. Hotchi, K. Imai, E.H. Kim, J.H. Kim, T. Kishimoto, A. Krutenkova, K. Maeda, T. Nagae, M. Nakamura, H. Outa, T. Saito, A. Sakaguchi, Y. Sato, R. Sawafta, M. Sekimoto, Y. Shimizu, T. Takahashi, H. Tamura, L. Tang, K. Tanida, T. Watanabe, H.H. Xia, S.H. Zhou, X.F. Zhu, L.H. Zhu, Phys. Rev. C 70 (2004) 044613.

[46] Y. Sugahara, H. Toki, Nucl. Phys, A 579 (1994) 557.

[47] V.K. Magas, E. Oset, A. Ramos, H. Toki, *A critical view on the deeply bound K^-pp system*, arXiv:nucl-th/0601013.

[48] J. Yamagata, H. Nagahiro, Y. Okumura, S. Hirenzaki, Prog. Theor. Phys. 114 (2005) 301; and Erratum, ibid. 905.